Current Biology 20, 939–943, May 25, 2010 ©2010 Elsevier Ltd All rights reserved DOI 10.1016/j.cub.2010.03.065

Report

Neck Linker Length Determines the Degree of Processivity in Kinesin-1 and Kinesin-2 Motors

Shankar Shastry[1] and William O. Hancock[1,*]
[1]Department of Bioengineering, The Pennsylvania State University, 205 Hallowell Building, University Park, PA 16802, USA

Summary

Defining the mechanical and biochemical determinates of kinesin processivity is important for understanding how diverse kinesins are tuned for specific cellular functions. Because transmission of mechanical forces through the 14–18 amino acid neck linker domain underlies coordinated stepping [1–6], we investigated the role of neck linker length, charge, and structure in kinesin-1 and kinesin-2 motor behavior. For optimum comparison with kinesin-1, the KIF3A head and neck linker of kinesin-2 were fused to the kinesin-1 neck coil and rod. Extending the 14-residue kinesin-1 neck linker reduced processivity, and shortening the 17-residue kinesin-2 neck linker enhanced processivity. When a proline in the kinesin-2 neck linker was replaced, kinesin-1 and kinesin-2 run lengths scaled identically with neck linker length, despite moving at different speeds. In low-ionic-strength buffer, charge had a dominant effect on motor processivity, which resolves ongoing controversy regarding the effect of neck linker length on kinesin processivity [3, 5–7]. From stochastic simulations, the results are best explained by neck linker extension slowing strain-dependent detachment of the rear head along with diminishing strain-dependent inhibition of ATP binding. These results help delineate how interhead strain maximizes stepping and suggest that less processive kinesins are tuned to coordinate with other motors differently than the maximally processive kinesin-1.

Results and Discussion

Extending the Kinesin-1 Neck Linker Decreases Processivity

To investigate the influence of neck linker length on kinesin-1 processivity, we visualized homodimeric *Drosophila* conventional kinesin, truncated at residue 559 and fused to a C-terminal GFP, moving along immobilized bovine brain microtubules by single-molecule total internal reflection fluorescence (TIRF) microscopy. To minimize any electrostatic tethering between the motor and microtubule that can complicate the interpretation of mechanical processivity, we performed experiments in 80 mM PIPES buffer. The control Kin1 motor moved at 990 ± 130 nm/s (mean ± standard deviation), with a mean run length of 2.1 ± 0.1 μm (mean ± standard error of fit) (Figure 1A). When the neck linker domain was extended by three residues ($Kin1_{+DAL}$, corresponding to the last three residues of the kinesin-2 neck linker), the run length dropped by a factor of five to 0.39 ± 0.02 μm and the speed dropped to 600 ± 89 nm/s. Interestingly, inserting only one amino acid ($Kin1_{+L}$) diminished the run length to 0.89 ± 0.06 μm and the speed to 580 ± 95 nm/s (Figure 1B). Finally, shortening the neck linker by one residue ($Kin1_{\Delta T}$) abolished processivity (see Supplemental Results and Discussion and Figure S1 available online). These results confirm and extend previous work with full-length kinesin attached to beads [6] and demonstrate that kinesin-1 processivity is significantly reduced when the neck linker domain is extended by even one amino acid.

Shortening the Kinesin-2 Neck Linker Enhances Processivity

The intraflagellar transport motor kinesin-2 has a 17 amino acid neck linker, three residues longer than kinesin-1, and in previous work we showed that full-length kinesin-2 is 4-fold less processive than kinesin-1 [6]. If the reduced processivity of kinesin-2 results from diminished coordination between the heads that results from its longer neck linker domain, then a simple prediction is that shortening the kinesin-2 neck linker domain should enhance processivity. To test this, we made a motor consisting of the head and neck linker of the mouse KIF3A subunit of kinesin-2 (ending in the last residue of the neck linker domain, Leu359) fused to the neck coil and proximal rod of *Drosophila* kinesin-1 (starting at the first residue of the neck coil domain, Ala345) (Figure 1C). This kinesin-2 construct was used so that any differences in processivity can be attributed solely to the head and neck linker regions, and not to differences such as charge or mechanical integrity of the coiled coil. Whereas constructs containing the kinesin-2 coiled coil were only functional when they were baculovirus-expressed, these kinesin-1/kinesin-2 chimeras were functional when bacterially expressed and had similar properties to a baculovirus-expressed KIF3A homodimer investigated previously [6]. These GFP-tagged chimeric constructs are referred to as Kin2 throughout this paper.

The mean run length and speed of control Kin2 were 0.71 ± 0.03 μm and 480 ± 98 nm/s, respectively. To test whether shortening the neck linker enhances processivity, we made stepwise deletions of one, two, and three amino acids in the last three residues (DAL) in the kinesin-2 neck linker to create $Kin2_{\Delta A}$, $Kin2_{\Delta DA}$, and $Kin2_{\Delta DAL}$. Single-molecule run lengths and velocities were measured in a manner identical to Kin1. Deleting one residue ($Kin2_{\Delta A}$) increased the run length to 1.26 μm and had no effect on the velocity (484 nm/s), supporting the hypothesis. However, deleting two residues ($Kin2_{\Delta DA}$) decreased the mean run length to 0.59 μm, which is less than the control Kin2 motor. Deleting all three residues ($Kin2_{\Delta DAL}$) resulted in no observable processive runs in the single-molecule assay (Figure 2C), though the motors were functional in the multimotor gliding assay (Supplemental Results and Discussion and Table S2). Hence, although the results qualitatively agree with the hypothesis—shortening the kinesin-2 neck linker enhances processivity—there was not quantitative agreement between the kinesin-1 and kinesin-2 results.

Both KIF3A and KIF3B contain a proline residue at position 13 of the neck linker domain (Figure 1C), and in the only kinesin-2 crystal structure containing the entire neck linker domain (human KIF3B; Protein Data Bank ID code 3B6U), this proline is

*Correspondence: wohbio@engr.psu.edu

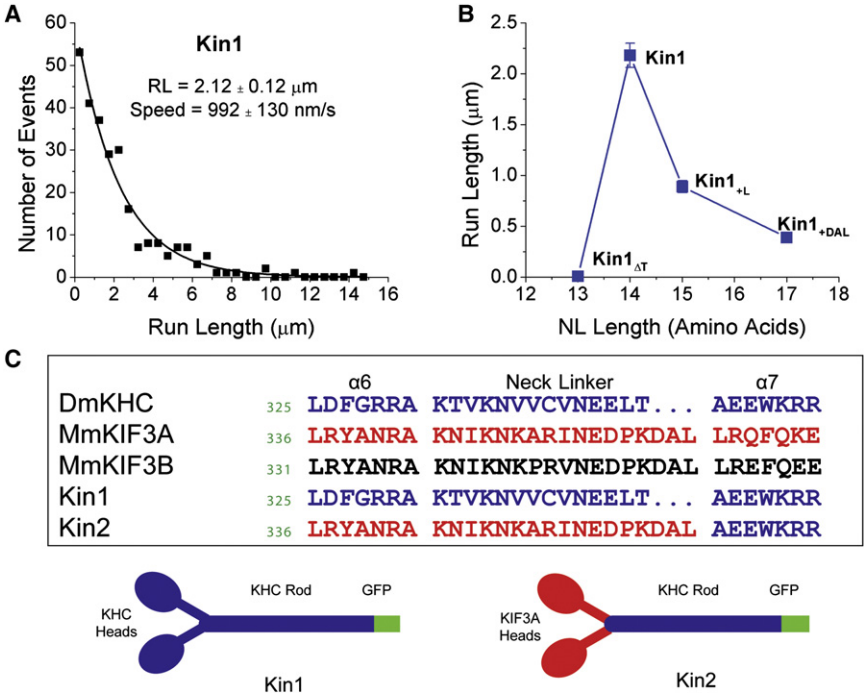

Figure 1. Kin1 Run Lengths and Design of Kin1 and Kin2 Constructs

(A) Run length of control Kin1 from total internal reflection fluorescence assay. Data were fit to a single exponential.

(B) Run lengths of different Kin1 constructs as a function of their neck linker (NL) length. Error bars represent the standard error from exponential fits.

(C) Amino acid sequence of the kinesin-1 (KHC) and kinesin-2 (KIF3A) neck linkers with the adjacent α6 (last helix in the head domain) and α7 (neck coiled-coil domain). The Kin1 construct includes the entire DmKHC sequence up to residue 559 (in the break between coil 1 and coil 2 of the rod domain [19]) followed by a C-terminal GFP and His_6 tag. The Kin2 construct includes the KIF3A head and 17-residue neck linker domain ending at Leu359 (red sequence) fused to the DmKHC neck coil and rod, starting at Ala345, the first residue in the neck coil domain (dark blue sequence). The cartoon shows the structures of the Kin1 and Kin2 constructs. The neck linker sequences for all constructs used are given in Table S1.

in the kinked *cis* conformation. We used molecular dynamics simulations to compare the predicted force-extension profiles of kinesin-1 and kinesin-2 neck linkers and found that, whereas the kinesin-1 neck linker was well fit by a model of a 14-residue worm-like chain, the 17-residue kinesin-2 neck linker was shorter than predicted by a worm-like chain model, except at high forces where the proline was forced into the straight *trans* conformation [8] (Figure 2A). When the proline at position 13 was changed to an alanine and the last three residues of the kinesin-2 neck linker were deleted, the modeled force-extension curve matched that of kinesin-1 (Figure 2B).

Kin1 and Kin2 Motor Properties Scale Similarly with Neck Linker Length

Motivated by these molecular dynamics simulations, we substituted the proline at position 13 of the Kin2 neck linker with alanine ($Kin2_{PA}$) and found that the mean run length fell from 0.71 μm to 0.39 μm, consistent with this substitution extending the effective neck linker length. Interestingly, the processivity of this $Kin2_{PA}$ construct closely matched that of the equivalent kinesin-1 construct, $Kin1_{+DAL}$ (0.39 μm) (Figure 2D; Table S2). More importantly, when the neck linker of this proline-substituted construct was shortened by three

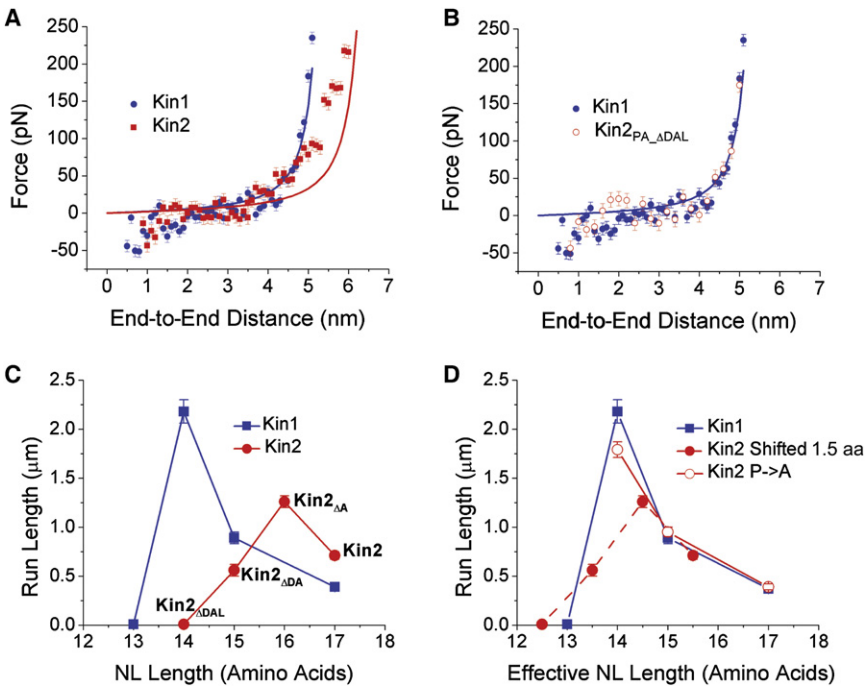

Figure 2. Kin1 and Kin2 Run Lengths Scale with Neck Linker Length

(A) Force-extension curves of kinesin-1 and kinesin-2 neck linkers from molecular dynamics simulations. Solid lines are predictions of a worm-like chain model for 14- and 17-residue polypeptides showing good fit for kinesin-1 (14 residues) and poor fit for kinesin-2 (17 residues). Data are replotted from [8].

(B) Predicted force-extension curve when the kinked proline in kinesin-2 is replaced with an alanine and the last three amino acids are deleted ($Kin2_{PA\_\Delta DAL}$), compared to kinesin-1.

(C) Comparison of run lengths for Kin2 and Kin1 constructs with identical neck linker lengths (number of amino acids).

(D) Run lengths following substitution of the *cis* proline in the Kin2 neck linker with alanine ($Kin2_{PA}$). $Kin2_{PA}$ constructs containing 14-, 15-, and 17-residue neck linkers are $Kin2_{PA\_\Delta DAL}$, $Kin2_{PA\_\Delta DA}$, and $Kin2_{PA}$, respectively. The curve for control Kin2 motors is shifted 1.5 amino acids to the left to account for the *cis* proline. All run length and velocity values are given in Table S2.

residues to match the length of the kinesin-1 neck linker, the mean run length of this Kin2$_{PA_\Delta DAL}$ construct rose to 1.8 μm, more than twice the native Kin2 processivity and very nearly matching the 2.1 μm run length of wild-type Kin1 (Figure 2D). To further examine this correlation, we then made an intermediate length construct, Kin2$_{PA_\Delta DA}$, containing a 15-residue neck linker domain and found that its run length closely matched the kinesin-1 construct having a 15-residue neck linker, Kin1$_{+L}$. The striking result here is that when the kinesin-2 neck linker is straightened by removing the *cis* proline, the run lengths of kinesin-1 and kinesin-2 motors match and scale similarly with neck linker length even though motor velocities remain distinct. As an example, the run lengths of Kin1 and Kin2$_{PA_\Delta DAL}$ are nearly identical, although their motor velocities differ by nearly a factor of two (990 ± 130 nm/s versus 508 ± 71 nm/s).

To extend this correlation of processivity with neck linker length, it is possible to estimate the degree to which the proline in the *cis* conformation shortens the kinesin-2 neck linker. Shortening the Kin2 neck linker by one residue increases processivity, whereas shortening it by two residues diminishes processivity and shortening it by three abolishes processivity altogether (Figure 2C). This is consistent with the maximum predicted run length lying between a deletion of one and two residues. When the Kin2 curve is shifted to the left by 1.5 amino acids, all three curves fall on top of one another (Figure 2D), suggesting that the kinked proline shortens the neck linker domain by the equivalent of 1.5 amino acids (~0.5 nm).

Adding Positive Charge in the Neck Linker Enhances Processivity

Although it is clear that neck linker length controls processivity, the degree to which charged residues in the neck linker also affect processivity is not clear. Positively charged residues in the neck coil domain and in the core head domain have been shown to enhance processivity through favorable electrostatic interactions with the microtubule [9, 10]. Understanding the dependence of kinesin processivity on neck linker charge and buffer ionic strength is important for properly interpreting the present data and for resolving disparate results in the literature. To test the extent to which the reduced run length of Kin1$_{+DAL}$ is due to unfavorable electrostatic interactions caused by the negative charge of the insert (−1 at physiological pH), we instead inserted a neutral three-residue insert, AAL. Kin1$_{+AAL}$ had a similar run length (0.45 μm; Figure 3A), confirming that the DAL insert reduces processivity by lengthening the neck linker and not by introducing negative charge. In contrast, extending the neck linker with a positively charged insert, KAL (Kin1$_{+KAL}$), resulted in a run length of 1.27 μm, which is more than 2-fold greater than Kin1$_{+DAL}$ or Kin1$_{+AAL}$ but is still considerably less processive than Kin1 (2.1 μm) (Figure 3A). Hence, even in 80 mM PIPES buffer, positively charged residues in the kinesin neck linker domain enhance processivity. However, in this case, the reduction in processivity due to lengthening the neck linker still clearly dominates over any electrostatic effects from the positively charged lysine.

If electrostatic interactions are playing a role in kinesin processivity, then the effect should be magnified in low-ionic-strength buffers where charge shielding is minimized. To test the effect of ionic strength on kinesin processivity, we measured run lengths of Kin1 and Kin1$_{+KAL}$ in 12 mM PIPES buffer and compared the values to run lengths in 80 mM PIPES buffer. In 12 mM PIPES, the Kin1 run length doubled to 4.2 μm and the Kin1$_{+KAL}$ run length increased 4-fold to 4.6 μm, such that the Kin1 and Kin1$_{+KAL}$ run lengths were nearly identical (Figure 3B). Hence, in low-ionic-strength buffers, the reduction in processivity resulting from extending the neck linker was almost perfectly matched by the enhancement in processivity resulting from the positively charged lysine in the insert.

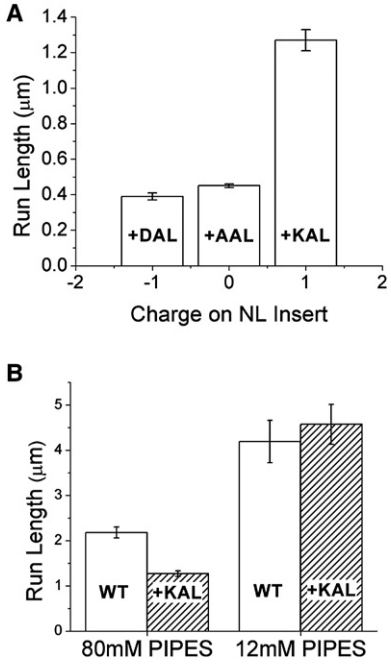

Figure 3. Neck Linker Positive Charge and Low Ionic Strength Enhance Processivity

(A) Kin1 run length as a function of the charge of the neck linker insert, showing that although negative charge does not diminish processivity, adding positive charge does enhance processivity. Experiments were carried out in 80 mM PIPES buffer.

(B) Effect of buffer ionic strength on control Kin1 and Kin1$_{+KAL}$ run lengths, showing that in 12 mM PIPES buffer, the diminished processivity due to the longer neck linker domain is compensated for by enhanced electrostatic interactions due to the added positive charge in the neck linker domain.

This finding that charge introduced in the neck linker plays a dominating role at low ionic strength helps to resolve the disparity between the present data and the results of Yildiz et al. [5], who found that inserts doubling the neck linker length had no significant effect on processivity. In that work, every insert in the neck linker contained an additional two lysines and a glycine; the authors argued that these positive charges compensated for moving the normal positive charge in the neck coil domain farther from the microtubule. Based on our results, the enhanced electrostatic interactions from these two lysines, which will be amplified in the 12 mM PIPES buffer used in that study, overwhelmed any reduction in processivity resulting from extending the neck linker domains. The simplest explanation is that these positively charged residues enhance processivity by interacting with the negatively charged C terminus of tubulin [9–11], although other mechanisms cannot be ruled out. We argue that for understanding the chemomechanical coordination between the two head domains that underlies kinesin processivity, these electrostatic effects should be minimized by using higher-ionic-strength buffers and minimizing positive charge in any sequence inserts.

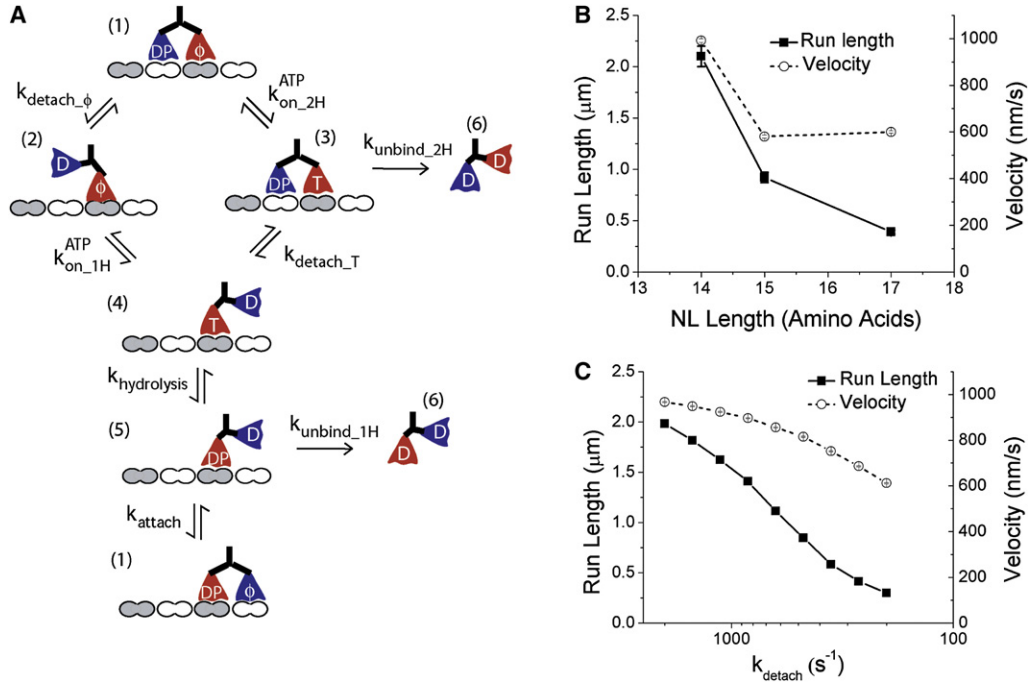

Figure 4. Modeling the Kinesin Chemomechanical Cycle

(A) Model for the kinesin chemomechanical cycle used to interpret the neck linker extension results. This framework is similar to a previous model [6], with the difference that motor unbinding from state 3 is combined into one rate constant (k_{unbind_2H}) for simplicity. Kinetic parameters are discussed in Supplemental Results and Discussion and listed in Table S3.

(B) Experimental Kin1 run length and velocity results, plotted as a function of neck linker length.

(C) Modeled run length and velocity from stochastic simulations of the model presented in (A), using rate constant parameters given in Table S3. In these simulations, $k_{on\_ATP\_2H}$ was set to 0.2 $\mu M^{-1}s^{-1}$ (10-fold above the best estimate from the literature [2]) and both k_{detach_φ} and k_{detach_T} were varied from 2000 s^{-1} down to 200 s^{-1} to model the effect of reduced strain on the trailing head due to extending the neck linker domain. Hence, for the model to account for the experimental results, extending the neck linker needs to alter two strain-dependent mechanisms—detachment of the trailing head and ATP binding to the leading head. Additional simulation results are given in Figure S4.

How Does Extending the Neck Linker Alter the Kinesin Chemomechanical Cycle?

To understand the mechanism by which extending the kinesin neck linker reduces processivity by a factor of five while reducing velocity less than 2-fold, we carried out stochastic simulations of the kinesin-1 kinetic cycle (Figure 4A) to identify whether modifications of individual model parameters are sufficient to account for the experimental results. Kinesin processivity is described by two mechanisms, front-head and rear-head gating [2, 4, 6]. Front-head gating holds that when both heads are bound (state 1), ATP binding to the leading head is inhibited by rearward strain, ensuring that the trailing head detaches before ATP binds (state 2). Rear-head gating holds that detachment from a one-head-bound state (state 5) is slow and forward-directed strain from the second head is necessary to detach the rear head (state 1 to 2 or state 3 to 4) at a rate consistent with the overall cycle time [4, 12].

For wild-type kinesin-1, where front-head gating is thought to block state 3 [2], processivity is determined by the relative rates of unbinding of the attached head (state 5 to state 6) versus rebinding of the tethered head (state 5 to state 1). To test whether changes in k_{attach} alone can account for the experimental results, we ran simulations at a range of k_{attach} values while holding all other parameters constant. Depending on the specific parameters used, the experimental results could be accounted for by positing that extending the neck linker reduces k_{attach} (Figure S4; Table S3). However, because attachment involves tethered diffusion of the unbound head, constrained by the entropic elasticity of the neck linker [6, 8, 13], extending the neck linker would be expected if anything to increase k_{attach} rather than decrease it. Nonetheless, this mechanism remains a formal possibility.

The next mechanism tested was the possibility that extending the kinesin-1 neck linker disrupts front-head gating by increasing the ATP binding rate in the two-head-bound state (state 1 to state 3 transition). To test whether a change in ATP binding alone is sufficient to account for the data, we varied $k_{on\_ATP\_2H}$ from 0.02 $\mu M^{-1}s^{-1}$ (consistent with experimental estimates in the strained state [2]) to 2 $\mu M^{-1}s^{-1}$ (the unstrained rate [2, 14]). A steep fall in run length was indeed observed, but velocity was unchanged (Figure S4). Hence, although this proposed mechanism can account for the effect of neck linker extension on run length, it cannot account for changes in velocity.

The third mechanism tested was the possibility that extending the neck linker domain slows strain-induced detachment of the trailing head. This strain-dependent detachment not only underlies rear-head gating, it also underlies front-head gating—detachment of the trailing head in state 1 must be very fast to prevent ATP binding to the front head and possible detachment from state 3. Depending on the rate constants chosen, decreasing the strain-induced detachment of the rear head (an expected outcome of lengthening the neck

linker) does result in a steep fall in run length and a moderate decrease in velocity (Figure 4C). However, this result is dependent on setting $k_{on\_ATP\_2H}$ to a value 10-fold faster than the experimentally estimated rate [2], setting k_{detach} to be very fast (2000 s^{-1}), and setting the unbinding rate from the two-head-bound state 3 to be 10-fold faster than the one-head-bound unbinding rate (state 5) (Table S3). Hence, changing either the ATP binding rate alone or the strain-dependent detachment rate of the trailing head alone fails to account for the experimental results. Instead, the neck linker extension results are best accounted for by both a slowing of the strain-dependent detachment rate k_{detach} and an increase in the strain-suppressed two-headed ATP binding rate $k_{on\_ATP\_2H}$.

The striking finding of this study is that virtually all of the difference in processivity between kinesin-1 and kinesin-2 motors results from differences in the length of the neck linker domain, and not from inherent differences in kinetic rates in the heads. Hence, when Kin1 and Kin2 neck linkers are identical lengths (following proline substitution), their run lengths match despite the fact that motor velocities differ by nearly a factor of two. The results can be accounted for by proposing that extending the neck linker both decreases strain-induced detachment of the trailing head (k_{detach}) and relieves the strain-inhibited binding of ATP to the leading head in the two-head-bound state. Because internal strain between the heads in kinesin-2 motors is less than in kinesin-1, it is expected that kinesin-2 responds differently to external strain such as during bidirectional transport of cargo or when many motors are cooperatively transporting cargo. Sequence predictions indicate that motors in different kinesin families have different neck linker lengths [8], and they are known to possess different degrees of processivity and work in diverse multi-motor arrangements; hence, this correlation of neck linker length with their cellular task may extend across the kinesin superfamily.

Experimental Procedures

Motor Constructs and Protein Expression

Kin1 was made by fusing *Drosophila* conventional kinesin truncated at position 559 to a C-terminal eGFP and His_6 tag. Kin2 was engineered by swapping the head and neck linker of mouse KIF3A into Kin1 (Figure 1C). See Supplemental Experimental Procedures for details on cloning procedures and sequences. All motors were expressed in bacteria and purified by Ni column chromatography as described previously [15, 16].

Motility Assays

Bovine brain tubulin was purified and labeled with Cy5 (GE Healthcare) as described previously [16–18]. Taxol-stabilized Cy5-labeled microtubules were adsorbed onto the surface of flow cells, and the surfaces were blocked with 2 mg/ml casein. Motility solution consisting of ~20 pM motors, 1 mM MgATP, 0.2 mg/ml casein, 10 μM Taxol, 20 mM D-glucose, 0.02 mg/ml glucose oxidase, 0.008 mg/ml catalase, and 0.5% v/v β-mercaptoethanol in BRB80 (80 mM K-PIPES, 1 mM $MgCl_2$, 1 mM EGTA [pH 6.8]) was then introduced. Single-molecule run lengths were visualized by TIRF with a Nikon TE2000 microscope (60×, 1.45 NA Plan Apo) equipped with a 488 nm Ar ion laser for GFP excitation and a 633 nm He-Ne laser for Cy5 excitation; experiments were performed at 26°C. Images were captured with a Cascade 512 CCD camera (Roper Scientific), and acquisition and image analysis were carried out with MetaVue software (Molecular Devices); pixel size was 71.0 nm. The duration and distance of single motor runs were recorded manually. To ensure that all events were reliably captured, we only analyzed events with a minimum run length of 250 nm, and this minimum distance was subtracted from all runs (this assumes that detachment probability is independent of the distance that the motor has moved).

Supplemental Information

Supplemental Information includes Supplemental Results and Discussion, three tables, four figures, and Supplemental Experimental Procedures and can be found with this article online at doi:10.1016/j.cub.2010.03.065.

Acknowledgments

The authors thank V. Hariharan for work on molecular dynamics simulations and N. Jones for protein purification assistance. This work was supported by National Institutes of Health grant GM076476 to W.O.H.

Received: January 21, 2010
Revised: March 26, 2010
Accepted: March 29, 2010
Published online: May 13, 2010

References

1. Vale, R.D., and Milligan, R.A. (2000). The way things move: looking under the hood of molecular motor proteins. Science *288*, 88–95.
2. Rosenfeld, S.S., Fordyce, P.M., Jefferson, G.M., King, P.H., and Block, S.M. (2003). Stepping and stretching. How kinesin uses internal strain to walk processively. J. Biol. Chem. *278*, 18550–18556.
3. Hackney, D.D., Stock, M.F., Moore, J., and Patterson, R.A. (2003). Modulation of kinesin half-site ADP release and kinetic processivity by a spacer between the head groups. Biochemistry *42*, 12011–12018.
4. Block, S.M. (2007). Kinesin motor mechanics: binding, stepping, tracking, gating, and limping. Biophys. J. *92*, 2986–2995.
5. Yildiz, A., Tomishige, M., Gennerich, A., and Vale, R.D. (2008). Intramolecular strain coordinates kinesin stepping behavior along microtubules. Cell *134*, 1030–1041.
6. Muthukrishnan, G., Zhang, Y., Shastry, S., and Hancock, W.O. (2009). The processivity of kinesin-2 motors suggests diminished front-head gating. Curr. Biol. *19*, 442–447.
7. Miyazono, Y., Hayashi, M., Karagiannis, P., Harada, Y., and Tadakuma, H. (2009). Strain through the neck linker ensures processive runs: a DNA-kinesin hybrid nanomachine study. EMBO J. *29*, 93–106.
8. Hariharan, V., and Hancock, W.O. (2009). Insights into the mechanical properties of the kinesin neck linker domain from sequence analysis and molecular dynamics simulations. Cell. Mol. Bioeng. *2*, 177–189.
9. Thorn, K.S., Ubersax, J.A., and Vale, R.D. (2000). Engineering the processive run length of the kinesin motor. J. Cell Biol. *151*, 1093–1100.
10. Okada, Y., and Hirokawa, N. (2000). Mechanism of the single-headed processivity: diffusional anchoring between the K-loop of kinesin and the C terminus of tubulin. Proc. Natl. Acad. Sci. USA *97*, 640–645.
11. Lakämper, S., and Meyhöfer, E. (2005). The E-hook of tubulin interacts with kinesin's head to increase processivity and speed. Biophys. J. *89*, 3223–3234.
12. Hancock, W.O., and Howard, J. (1999). Kinesin's processivity results from mechanical and chemical coordination between the ATP hydrolysis cycles of the two motor domains. Proc. Natl. Acad. Sci. USA *96*, 13147–13152.
13. Hyeon, C., and Onuchic, J.N. (2007). Internal strain regulates the nucleotide binding site of the kinesin leading head. Proc. Natl. Acad. Sci. USA *104*, 2175–2180.
14. Hackney, D.D. (2002). Pathway of ADP-stimulated ADP release and dissociation of tethered kinesin from microtubules. Implications for the extent of processivity. Biochemistry *41*, 4437–4446.
15. Hancock, W.O., and Howard, J. (1998). Processivity of the motor protein kinesin requires two heads. J. Cell Biol. *140*, 1395–1405.
16. Uppalapati, M., Huang, Y.-M., Shastry, S., Jackson, T.N., and Hancock, W.O. (2009). Microtubule motors in microfluidics. In Methods in Bioengineering: Microfabrication and Microfluidics, J.D. Zahn, ed. (Boston, MA: Artech House Publishers), pp. 311–336.
17. Williams, R.C., Jr., and Lee, J.C. (1982). Preparation of tubulin from brain. Methods Enzymol. *85 Pt B*, 376–385.
18. Hyman, A., Drechsel, D., Kellogg, D., Salser, S., Sawin, K., Steffen, P., Wordeman, L., and Mitchison, T. (1991). Preparation of modified tubulins. Methods Enzymol. *196*, 478–485.
19. Coy, D.L., Hancock, W.O., Wagenbach, M., and Howard, J. (1999). Kinesin's tail domain is an inhibitory regulator of the motor domain. Nat. Cell Biol. *1*, 288–292.

Current Biology, Volume *20*

Supplemental Information

Neck Linker Length Determines the Degree of Processivity in Kinesin-1 and Kinesin-2 Motors

Shankar Shastry and William O. Hancock

Supplemental Results and Discussion

Table S1. Complete Neck Linker Sequences for Motors Used

		α6	Neck-linker	α7
Kin1	325	LDFGRRA	KTVKNVVCVNEELT...	AEEWKRR
$Kin1_{+L}$	325	LDFGRRA	KTVKNVVCVNEELTL..	AEEWKRR
$Kin1_{+DAL}$	325	LDFGRRA	KTVKNVVCVNEELTDAL	AEEWKRR
$Kin1_{+AAL}$	325	LDFGRRA	KTVKNVVCVNEELTAAL	AEEWKRR
$Kin1_{+KAL}$	325	LDFGRRA	KTVKNVVCVNEELTKAL	AEEWKRR
$Kin1_{\Delta T}$	325	LDFGRRA	KTVKNVVCVNEEL....	AEEWKRR
Kin2	336	LRYANRA	KNIKNKARINEDPKDAL	AEEWKRR
$Kin2_{\Delta A}$	336	LRYANRA	KNIKNKARINEDPKDL.	AEEWKRR
$Kin2_{\Delta DA}$	336	LRYANRA	KNIKNKARINEDPKL..	AEEWKRR
$Kin2_{\Delta DAL}$	336	LRYANRA	KNIKNKARINEDPK...	AEEWKRR
$Kin2_{PA}$	336	LRYANRA	KNIKNKARINEDAKDAL	AEEWKRR
$Kin2_{PA\_\Delta DA}$	336	LRYANRA	KNIKNKARINEDAKL..	AEEWKRR
$Kin2_{PA\_\Delta DAL}$	336	LRYANRA	KNIKNKARINEDAK...	AEEWKRR

The neck linker domain connects α6, the last helix of the motor domain to α7, the first helix of the dimerization domain. The definitions of the start and end of the neck linker were discussed previously [1,2]. Kin1 constructs include the control, extensions of 1 and 3 amino acids, and deletion of 1 amino acid. Kin2 constructs include the control motor and deletions of 1, 2 and 3 amino acids before and after substitution of Pro_{355} for Ala.

Table S2. Run Lengths and Velocities of All Kin1 and Kin2 Motors Used

Construct	Neck Linker Length (Amino Acids)	Run Length (μm) Mean ± SEM (N)	Speed (nm/s) Mean ± SD (N)
Kin1	14	2.1 ± 0.10 (263)	990 ± 130 (263)
$Kin1_{+L}$	15	0.89 ± 0.06 (168)	580 ± 95 (168)
$Kin1_{+DAL}$	17	0.39 ± 0.02 (339)	600 ± 89 (339)
$Kin1_{+AAL}$	17	0.45 ± 0.01 (197)	713 ± 127 (197)
$Kin1_{+KAL}$	17	1.27 ± 0.06 (319)	787 ± 100 (319)
$Kin1_{\Delta T}$	13	Non Processive	607 ± 86 (30)**
Kin2	17*	0.71 ± 0.03 (236)	480 ± 98 (236)
$Kin2_{\Delta A}$	16*	1.26 ± 0.06 (333)	484 ± 77 (333)
$Kin2_{\Delta DA}$	15*	0.59 ± 0.03 (190)	490 ± 98 (190)
$Kin2_{\Delta DAL}$	14*	Non Processive	353 ± 48 (27)**
$Kin2_{PA}$	17	0.39 ± 0.03 (105)	526 ± 92 (105)
$Kin2_{PA\_\Delta DA}$	15	0.95 ± 0.05 (165)	480 ± 88 (165)
$Kin2_{PA\_\Delta DAL}$	14	1.78 ± 0.08 (398)	508 ± 71 (398)

* Includes proline at position 13 in the neck linker
** Results from microtubule gliding assays where N is number of microtubules

Assessing the Processivity of $Kin1_{\Delta T}$ and $Kin2_{\Delta DAL}$

For processive kinesin stepping, there is presumably an optimum neck linker length—if the neck linker is too long it will be unable to transmit mechanical tension between the two head domains, but if it is too short, the tethered head won't be able to reach the next binding site on the microtubule. After finding that extending the kinesin-1 neck linker by one residue reduces processivity by half, we next tested the effect of shortening the neck linker by deleting Thr344, the last residue in the kinesin-1 neck linker. In high density microtubule gliding assays, $Kin1_{\Delta T}$ moved microtubules at 607 ± 86 nm/s. However, no processive events were observed in the single-motor TIRF assay.

We next explored $Kin1_{\Delta T}$ processivity using a bead assay. Full-length $Kin1_{\Delta T}$ motors were expressed and adsorbed to casein-coated 0.56 μm polystyrene beads as previously described[2]. Microtubules were adsorbed to flow cells and motility solution consisting of motor coated beads, 10 μM taxol, 1 mM ATP, 0.2 mg/ml casein and oxygen scavenging system in BRB80 was flowed in. Beads captured with a weak optical trap were

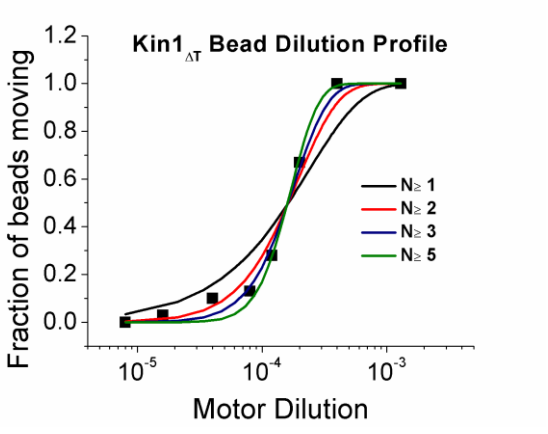

Figure S1. $Kin1_{\Delta T}$ Bead Dilution Profile
Fraction of beads that move when placed near an immobilized microtubule, plotted as a function of motor dilution. Data were fit best to a Poisson distribution with N ≥3, consistent with a non processive motor.

brought in contact with microtubules and bead movements were captured with the CCD camera[2].

To assess $Kin1_{\Delta T}$ processivity, the fraction of beads that moved when placed next to a microtubule was recorded at a range of motor concentrations (keeping the bead concentration constant). As seen in Figure S1, the fraction of moving beads fell steeply with motor dilution. The data were fit to a Poisson distribution as previously described[3], and the results were poorly fit by a curve with $N \geq 1$, and were best fit by a Poisson distribution with $N \geq 3$. This result confirms that $Kin1_{\Delta T}$ motors are indeed functional, but that they are minimally processive or nonprocessive.

While both the TIRF assay and the bead dilution profile of $Kin1_{\Delta T}$ suggested that the motors were non-processive, the upper limit of those measurements is approximately 200 nm, so they cannot say whether the motors are minimally processive (taking ~10 steps) or non-processive (taking only one step per interaction). Though motor runs shorter than 200 nm at 1 mM ATP were difficult to record reliably with the TIRF system, transient binding events at 2 µM ATP (where ATP binding is the rate limiting step) were observed. The residence times of these binding events were recorded and fit to an exponential, representing the motor off-rate from the microtubule. The mean duration was 1.60 ± 0.05 s (Figure S2A). In parallel, microtubule gliding assays with $Kin1_{\Delta T}$ were carried out at 2µM ATP. The measured gliding speed was 3.0 ± 0.1 nm/s.

Based on the 3 nm/s motor speed at 2 µM and the finding that individual motors interact with the microtubule for 1.6 s, the distance a motor moves per interaction is calculated to be 1.6 s * 3.0 nm/s = 4.8 ± 0.3 nm. This is less than one 8 nm step, and from this we conclude that $Kin1_{\Delta T}$ is not processive.

One caveat of this measurement is that the binding time is a single-molecule measurement, while the gliding speed is a manifestation of many motors working together. However, the motor detachment rate when many motors are moving a microtubule is, if anything, expected to be faster than in the single-molecule case due to forced unbinding. The binding duration and consequently the distance per interaction should be therefore be considered an upper limit, further supporting the conclusion that $Kin1_{\Delta T}$ is nonprocessive.

A similar set of measurements was carried out to assess the processivity of $Kin2_{\Delta DAL}$. The measured residence time at 2 µM ATP was 0.6 ± 0.05 s and gliding speed was 18 ± 0.4 nm/s,

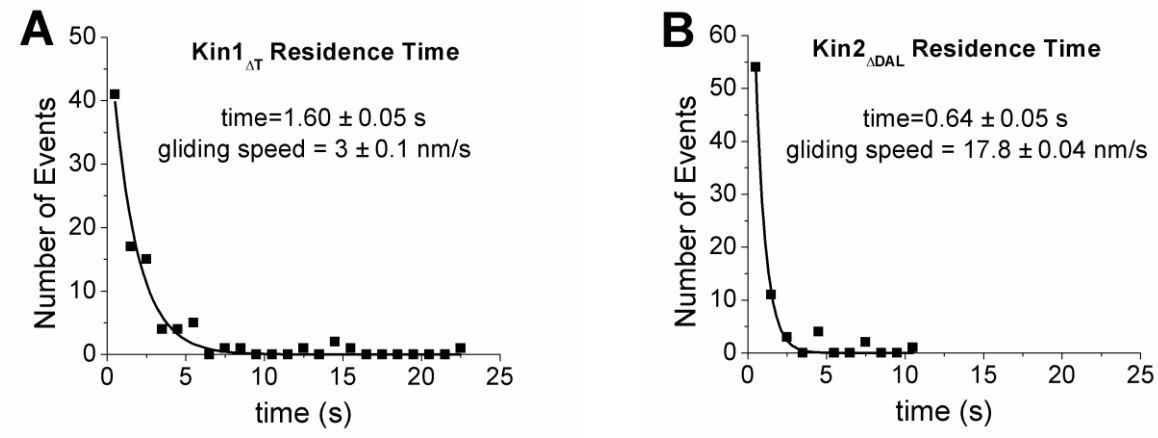

Figure S2. $Kin1_{\Delta T}$ and $Kin1_{\Delta DAL}$ Binding Events at 2 µM ATP

Binding times were binned in 1 second intervals and data were fit to a single exponential. Time is reported as fit ± SE of the fit. Motor speeds from microtubule gliding assays at 2 µM ATP are reported as mean ± SEM.

giving a predicted distance of 10.8 ± 1.1 nm per interaction with a microtubule. Although it can't be ruled out that $Kin2_{\Delta DAL}$ takes two steps (16 nm) per interaction, this motor is likely nonprocessive as well. The conclusion from these neck-truncated motors is that shortening the neck linker beyond a critical length either prevents the tethered head from reaching the next binding site or slows the binding rate to a degree that the motor detaches before the tethered head binds.

Stochastic Simulations of the Kinesin Chemomechanical Cycle

To test potential mechanisms by which extending the kinesin neck linker reduces processivity, we carried out stochastic simulations of the kinesin chemomechanical cycle with MATLAB. The structure of the model (Figure S3) and the modeling approach are similar to Muthukrishnan et al.[2], with the difference that motor unbinding from state 3 (following breakdown of front-head gating) is lumped into a single rate constant, k_{unbind_2H}. During stepping, transitions between adjacent states were calculated from the first-order rate constant using the Gillespie algorithm ($t = \frac{1}{k}\ln\frac{1}{rand\#}$) [4], and the fastest transition was chosen as the dwell time. For each simulation a motor starts in state 1 and steps through the cycle until it detaches from the microtubule, and the cycle time and distance moved (number of steps times 8 nm/step) are converted to run length and velocity. For each parameter set, 3000 motor runs were simulated.

The goal of these simulations was to test whether the observed dependence of run length and velocity on neck linker length can be explained by changes in a single parameter in the kinetic cycle. The governing philosophy is that the kinetic cycle is sufficiently complex that intuition breaks down and it is necessary to simulate the entire cycle to interpret the data. The simulations used the parameters used by Muthkrishnan et al.[2] as a starting point, and specific parameters were adjusted to better fit the data and test hypotheses for the effect of neck linker extension. Simulations focused on three parameters, k_{attach}, $k_{on\_ATP\_2H}$ and k_{detach}. To better understand the dynamics of the kinetic cycle, the relative flux through the two-head bound pathway (2H Path, Figure S3) was recorded, as well as the probability the motor unbound from the microtubule through the two-head bound state 3 rather than the one-head bound state 5.

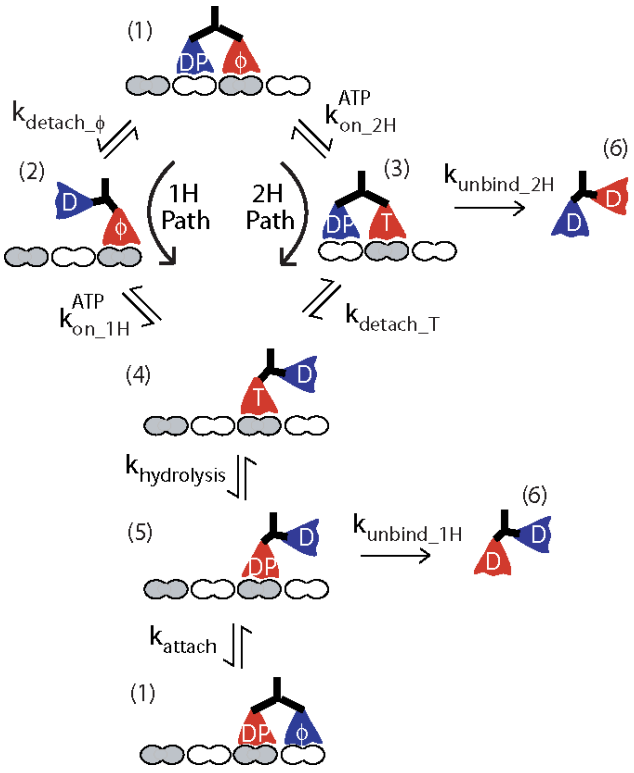

Figure S3. Kinesin Chemomechanical Model
Model describes the transitions in kinesin hydrolysis cycle, and is expanded from Figure 4A to show alternate paths for ATP binding or trailing head detachment from state 1.

Table S3. Rate Constants Used for Modeling Simulations

Rate Constants	Vary k_{attach}		Vary $k_{on\_ATP\_2H}$		Vary k_{detach}	
	Forward rate (s^{-1})	Backward rate (s^{-1})	Forward rate (s^{-1})	Backward rate (s^{-1})	Forward rate (s^{-1})	Backward rate (s^{-1})
k_{detach_ϕ}	250	0.01	250	0.01	2000	0.01
$k_{on\_ATP\_2H}$*[ATP]	20	20	20	20	200	20
$k_{on\_ATP\_1H}$	2000	20	2000	20	2000	20
k_{unbind_2H}	4		4		10	
k_{detach_T}	250	0.02	250	0.01	2000	0.01
$k_{hydrolysis}$	280	3.5	280	3.5	280	3.5
k_{unbind_1H}	4		4		1	
k_{attach}	1800	1.8	1200	1.2	280	0.28

Varying the attachment rate of the tethered head, k_{attach}

The first set of simulations tested whether the results can be explained by a change in k_{attach}, the rate that the tethered head binds to the microtubule (transition from state 5 to state 1). This is a key step because it is the primary path of detachment of the motor and the race between k_{attach} and k_{unbind_1H} determines the run length. Extending the neck linker domain is not expected to alter the motor unbinding rate, k_{unbind_1H}, but it is plausible that it could alter the rate at which the tethered head reattaches to the microtubule. The most reasonable expectation would be that extending the neck linker domain accelerates k_{attach} by loosening the tether of the unbound head, enabling its diffusion to the next binding site. However, in simulations where k_{attach} was increased, the run length increased, opposite of what is seen experimentally. Alternatively, it is formally possible that docking of the native neck linker places the tethered head in the optimal position for binding to the microtubule (despite the fact that the neck linker of the tethered head is expected to remain unstructured[5]), and extending the neck linker alters this positioning and consequently reduces the attachment rate. To simulate this possibility, k_{attach} was set to 1800 s^{-1} (which is necessary to prevent a significant reduction in motor velocity with decreases in k_{attach}, and which is generally consistent with the idea that neck linker docking of the bound head optimally positions the tethered head for attachment). k_{unbind_1H} was set to 4 s^{-1} to match observed run length of control Kin1, and k_{attach} was systematically reduced (entire parameter set given in Table S3). As seen in Figure S4A, reducing k_{attach} led to a significant drop in the run length and only a moderate fall in velocity, as seen experimentally. The flux analysis in Figure S4C helps to explain this behavior – decreasing k_{attach} does not alter the relative flux through the two pathways that emerge from state 1, but because it increases the probability of detaching from the one-head bound state 5, the fraction of motors that detach from the two-head bound state 3 falls.

Varying the ATP binding rate in the two-head-bound state, $k_{on\_ATP\_2H}$

The second set of simulations investigated whether the experimental results can be explained by the breakdown of front head gating – extending the neck linker leads to an increase in $k_{on\_ATP\_2H}$. The definition of front-head gating is that rearward strain on the front head in state 1 slows ATP binding, allowing time for the trailing head to detach (and preventing detachment via state 3). Hence, it is reasonable to propose that extending the length and thus the mechanical compliance

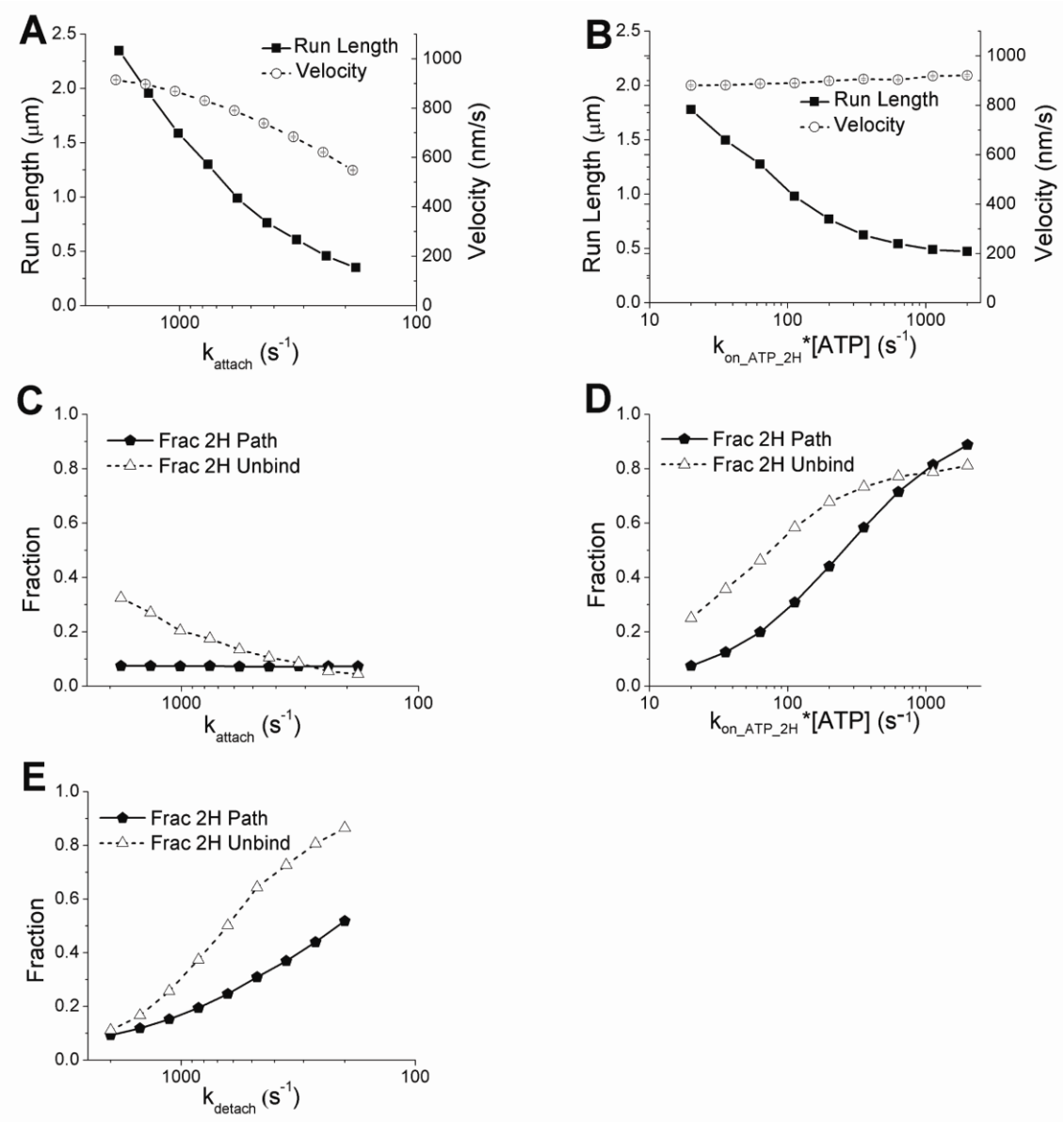

Figure S4. Run Length, Velocity, and Flux Analysis from Model Simulations
Simulations used rate constants shown in Table S3. (A and C) Run length and velocity results and flux analysis for simulations in which neck linker extension was modeled as a decrease in k_{attach}. (B and D) Run length and velocity results and flux analysis for simulations in which neck linker extension was modeled as an increase in $k_{on\_ATP\_2H}$. (E) Flux analysis for simulations in which neck linker extension was modeled as a decrease in k_{detach} (run length and velocity results for these simulations are presented in Figure 4C of the paper. For run length and velocity data, SEM bars (for 3000 simulated runs per point) are hidden in the symbols. ATP was set to 1 mM in all simulations.

of the neck linker domain should reduce the magnitude of this rearward tension and lead to an increase in $k_{on\_ATP\_2H}$. To test whether this proposal makes quantitative sense, $k_{on\_ATP\_2H}$ was increased from 0.02 $\mu M^{-1}s^{-1}$ up to 2 $\mu M^{-1}s^{-1}$, which matches the unstrained on-rate $k_{on\_ATP\_1H}$. In these simulations k_{attach} was 1200 s^{-1}, which is similarly fast as for the above k_{attach} simulations, and both motor unbinding rates were set to 4 s^{-1}. Rear head detachment (at 250 s^{-1}) and hydrolysis (280 s^{-1}) were co-rate limiting.

Decreasing $k_{on\_ATP\_2H}$ did lead to a sharp reduction in the motor run length, as seen in Figure S4B, but there was no change in velocity. The flux analysis in Figure S4D shows that decreasing $k_{on\_ATP\_2H}$ shunted the cycle through the 2H path, resulting in most motors detaching from the two-head bound state 3. Hence the run length data could be quantitatively explained by an increase in $k_{on\_ATP\_2H}$ due to reduced rearward strain, but the fall in velocity could not be explained by this modulation, so a change in $k_{on\_ATP\_2H}$ alone is not sufficient to explain the experimental results.

Varying the strain-dependent detachment rate of the trailing head, k_{detach}

The final set of simulations investigated whether the results can be accounted for by breakdown of front-head gating through a different mechanism – slowing of rear-head detachment. The definition of rear head gating is that unbinding from the one-head-bound state 5 is slow, and during the normal cycle, detachment of this trailing head is significantly accelerated by forward-directed strain caused by binding of the front head (state 1). Hence, it is reasonable to predict that extending the neck linker would slow this strain-dependent detachment. This slowing could reduce processivity because ATP would have time to bind to the leading head (state 3), leading to premature detachment via state 3. To test whether the experimental results can be explained solely by a slowing of k_{detach}, simulations were run keeping all parameters constant except k_{detach}.

The first problem that arose was that in the parameter sets used above for varying k_{attach} and $k_{on\_ATP\_2H}$ (Table S3), rear head detachment is partially rate limiting at 250 s^{-1}, and so any decrease in this rate constant reduces the velocity nearly proportionally. To resolve this problem, k_{detach} was increased to 2000 s^{-1} such that it was no longer rate limiting for the wild-type motor, and k_{attach} was reduced to 250 s^{-1} to maintain a similar overall cycle time. While this k_{detach} is quite fast, there are no experiments in the literature that clearly rule this out, and it is possible that the strain in this conformation is significant[1]. Using this parameter set, a second kinetic problem became apparent – using $k_{on\_ATP\_2H}$ of 0.02 $\mu M^{-1}s^{-1}$, which is consistent with the best experimental estimates of this parameter[6], the transition from state 1 to state 3 occurs at the relatively slow rate of 20 s^{-1} in 1 mM ATP. Hence, although decreasing k_{detach} did reduce the run length, it also led to significant slowing of the motor, contrary to what was seen experimentally.

The model was able to account for the experimental results provided: 1) detachment from the two-head-bound state 3 was relatively fast (k_{unbind_2H} = 10 s^{-1}), and 2) $k_{on\_ATP\_2H}$ was increased by a factor of 10 to 0.2 $\mu M^{-1}s^{-1}$. The parameter set for varying k_{detach} is presented in Table S3 and the results from these simulations are presented in Figure 4C of the paper. From the flux analysis in Figure S4E, it is clear one reason that k_{detach} reduces processivity is by increasing (by five-fold) the probability that the cycle will follow the 2H path. An additional reason that the fraction of motors detaching from state 3 increases so steeply is that following ATP binding to the front head, the rate that the rear head detaches from state 3 also decreases. What these simulations make clear is that using this model structure the observed experimental results cannot be solely explained by a decrease in k_{detach} with extensions of the neck linker domain. Instead, a change in a second strain-dependent parameter, $k_{on\_ATP\_2H}$, is needed to account for the data.

Supplemental Experimental Procedures

Details of Cloning Procedures

To make Kin2 constructs (mouse KIF3A fused to *Drosophila* Kinesin-1), a leucine was inserted into Kin1 at position 364 using Stratagene's Quick-Change II XL site-directed mutagenesis kit (catalog # 200521) to introduce the restriction site NheI. The KIF3A head and neck linker regions were then amplified and extended with restriction sites Nde1 and Nhe1 at the two ends, and the ends made sticky by digesting with Nde1 and Nhe1. Kin1-NheI plasmid was linearized with Nde1 and Nhe1 enzymes and ligated to the KIF3A head and neck linker sequence to yield the Kin2 construct. Kin1 extensions and Kin2 deletions and substitutions were incorporated using Stratagene's Quick-change II XL site-directed mutagenesis kit.

Molecular Dynamics Simulations of Neck Linker Force-Extension Curves

Molecular Dynamics simulations were carried out using Gromacs as described previously[1]. Simulations were run in constraint mode and included the last residue of α6 and the residue of α7 as "handles". Lines in Figure 2A and B are worm-like-chain force-extension profiles using a persistence length of 0.5 nm and a contour length of 0.38 nm per amino acid. For the $Kin2_{PA\_\Delta DAL}$ simulations in Figure 2B, the neck linker structure PDB:3B6U was modified by substituting the proline for an alanine and deleting the last three residues. Force values are mean ± SEM for a 160 ps simulation using 2 fs time steps.

Supplemental References

1. Hariharan, V., and Hancock, W.O. (2009). Insights into the mechanical properties of the kinesin neck linker domain from sequence analysis and molecular dynamics simulations. Cellular and Molecular Bioengineering *2*, 177-189.
2. Muthukrishnan, G., Zhang, Y., Shastry, S., and Hancock, W.O. (2009). The processivity of kinesin-2 motors suggests diminished front-head gating. Curr Biol *19*, 442-447.
3. Block, S.M., Goldstein, L.S., and Schnapp, B.J. (1990). Bead movement by single kinesin molecules studied with optical tweezers. Nature *348*, 348-352.
4. Gillespie, D.T. (1977). Exact stochastic simulation of coupled chemical reactions. J. Phys. Chem. *81*, 2340-2361.
5. Rice, S., Lin, A.W., Safer, D., Hart, C.L., Naber, N., Carragher, B.O., Cain, S.M., Pechatnikova, E., Wilson-Kubalek, E.M., Whittaker, M., et al. (1999). A structural change in the kinesin motor protein that drives motility. Nature *402*, 778-784.
6. Rosenfeld, S.S., Fordyce, P.M., Jefferson, G.M., King, P.H., and Block, S.M. (2003). Stepping and stretching. How kinesin uses internal strain to walk processively. J Biol Chem *278*, 18550-18556.